

Chapter 2

Local Oxidation Using Dynamic Force Mode: Toward Higher Reliability and Efficiency

Hiromi Kuramochi and John A. Dagata

Abstract Local oxidation by scanning probe microscopy (SPM) is used extensively for patterning nanostructures on metallic, insulating, and semiconducting thin films and substrates. Numerous possibilities for refining the process by controlling charge density within the oxide and shaping the water meniscus formed at the junction of the probe tip and substrate have been explored by a large number of researchers under both contact mode (CM) and dynamic-force mode (DFM) conditions. This article addresses the question of whether or not the oxide growth rate and feature size obtainable by each method arise from distinctly different kinetic processes or arise simply because charge buildup and dissipation evolve over different time scales for these two cases. We report simultaneous oxide-volume and current-flow measurements for exposures performed by CM and DFM and then go on to discuss the practical realization of enhanced reliability and energy efficiency made possible by a better understanding of the relation between oxidation time and ionic diffusion using DFM.

Keywords Meniscus formation · Oxidation time · Probe speed

2.1 Introduction

Local oxidation by scanning probe microscopy (SPM) [1] is a method for generating deliberate nanoscale patterns on a wide variety of substrates [See References 2–4 for reviews]. The fundamental principle of local oxidation is quite straightforward: A voltage applied between a conductive SPM tip and (positively biased) substrate, results in the formation of a highly non-uniform electric field, E , in the range of 10^8 V/m to 10^9 V/m. The E field attracts a stable water meniscus to the tip-sample junction, creates oxyanions from water molecules, and transports these oxyanions through the growing oxide film. At these field strengths almost all materials undergo reaction with oxygen anions. This simple scheme leads to oxidation of the substrate

H. Kuramochi (✉)

MANA, NIMS, Tsukuba 305-0044, Japan; NRI, AIST, Tsukuba 305-8568, Japan
e-mail: kuramochi.hiromi@nims.go.jp

on a scale determined by the dimensions of the *nanocell* defined by the water meniscus [5, 6]. Size, shape, and stability of the nanocell, in addition to the properties of the E field, are therefore of crucial importance for successful nanolithography using local oxidation.

This leads to a classification of oxidation conditions into four basic categories: In the simplest implementation, the properties of the nanocell are determined by the spontaneous occurrence of a water meniscus when by the probe tip is in direct contact with a substrate, i.e., the microscope is operated in contact mode (CM); conversely, if the microscope is operated in dynamic-force mode (DFM), variation of the oscillation amplitude and tip-sample separation offer alternative strategies for forming and maintaining the water meniscus during tip positioning and lithographic exposure. In addition, the E field may be constant for the duration of the voltage pulse, i.e., the applied voltage and tip-sample separation are both constant (DC), or may be varied by employing a voltage modulated waveform (VM). In contact mode, the E field is then variable if a voltage waveform rather than a constant pulse is imposed. On the other hand, modulation of the E field by both voltage waveform and the oscillation of the tip becomes possible with DFM, enabling both the shaping of the nanocell and ion current flow to be controlled either independently or in a synchronized manner over a wide range of time scales.

In the present work we demonstrate that the relationship between current density and oxide formation is essentially identical for CM and DFM exposure. We do so by re-examining space-charge and water-bridge formation concepts – notions which have been largely treated separately in the past – in a coherent and consistent fashion. A significant implication of this result is that all of the most critical aspects of the oxidation process can be optimized by controlling meniscus lifetime in the DFM operating mode using principles established from the extensive kinetics studies done more conveniently in contact mode. This more inclusive view of the four basic modes of local oxidation allows us to better understand some of the parameter choices for DFM operation reported previously in the literature.

In striking a proper balance between oxidation time and ionic diffusion, this understanding points the way toward achieving *maximum reliability*, defined as the success rate of writing deliberate, continuous features, and *energy efficiency*, defined as operating as close as possible to the transition point between transient and steady-state growth. From the standpoint of practical application, these are the primary metrics for the implementation of DFM approaches to local oxidation.

2.2 Kinetics of Space Charge Buildup and Water Bridge Formation

2.2.1 Space Charge Buildup

Local oxidation by SPM is an example of a reaction-diffusion system [7, 8]. The simplest kinetic description of such a system is a pair of first-order, coupled reaction

rates. As Alberty & Miller have shown [9], this simple system can be solved analytically to obtain expressions for the overall rate constants that describe the initial distribution of oxyanion binding sites in silicon and on the internal rearrangement of trapping defects as the oxide grows. Since the reaction occurs at low, i.e., room, temperature in a concentrated solid phase, reactants and products are not thermally equilibrated and time evolution of oxide is sub-diffusional. The extensive theoretical work of Plonka on dispersive kinetics for low-temperature, condensed phase systems addresses the time-dependent reactivities of a system not in thermal equilibrium with its environment [7]. The notion of anomalous diffusion [8] refers to the non-Gaussian propagation (in statistical physics terms) of the oxidation wave front through the substrate and depends on the initial distribution of oxyanion binding sites in silicon and on the internal rearrangement of trapping defects as the oxide grows. In particular, we have shown how Plonka's approach to time-dependent rate coefficients provides an excellent fit to experimental data for silicon over seven decades of time in air [10].

This approach is also consistent with the concepts of Uhlig [11] regarding the necessity of nonuniform charge distributions in the oxide film and the distinctions drawn by Fehlner & Mott about low-temperature oxidation [12]. These fundamental ideas form the basis for the subsequent description of silicon oxidation developed Wolters and Zegers-van Duynhoven [13] and Dubois & Bubbendorff [14] and us [10, 15–18]. Recent work by Kinser et al. [19] has extended this kinetic model to describe SPM oxidation of silicon in inert, organic solvents as well.

The oxide growth model for silicon is based on two assumptions, coupled kinetic pathways and time-dependent rate constants. Coupled kinetic pathways recognize that more than one reaction channel contributes to the overall growth rate. The first reaction channel represents the direct conversion of silicon and oxygen ions into oxide. The second channel corresponds to the build up of space charge defects in the oxide [15–17]. We imagine that local oxidation of silicon consists of the simplest possible example of coupled rate equations by considering a “direct” reaction represented by $A \rightarrow C$, with a first order rate constant k_4 , and an “indirect” one, $A \rightarrow B \rightarrow C$, with successive rate constants k_1 and k_3 [10]. (Systems of coupled, first-order reaction rate equations were first solved by Alberty & Miller [9]. Numbering of rate constants follows their scheme.) Initial conditions are set such that $A(t = 0) = [A_o]$, $B(t = 0) = C(t = 0) = 0$, where A_o represents the initial reactant concentration of single-crystal silicon and oxygen; $B(t)$ represents an intermediate, defected SiO_x slows the transport of oxyanions; and $C(t)$ represents the local oxide in its final state, close to the density of SiO_2 . However, simply applying this scheme on its own does not provide a quantitative fit to experimental data. This problem was encountered by Orians et al. [5] in their recent computational modelling effort. The source of this discrepancy has been treated in great detail by Plonka [7]: Low-temperature, condensed phase systems that are unable to achieve equilibrium with their environment exhibit time-dependent reactivity, i.e., the rate “constants” are not constant at all, but are strongly time-dependent. This means that local oxidation cannot be treated as a series of static steps since the system does not return to equilibrium, or “re-set”, on a time scale comparable to the integrated

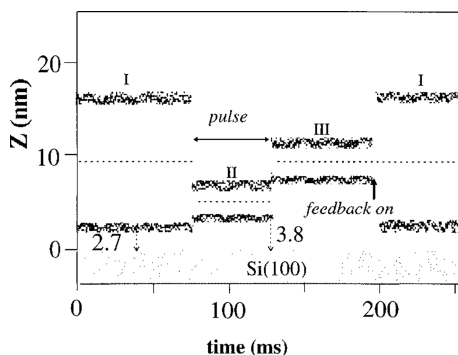
exposure time. In the case of first-order rate processes, time dependence adds a factor $t^{\alpha-1}$ such that the propagation of the oxidation wave front through the substrate depends on both the initial distribution of binding sites in the substrate and the increasingly disordered internal rearrangements of trapping defects as the oxide grows. This is referred to as *anomalous diffusion* [8] since its effect is to reduce wave front propagation from the $t^{1/2}$ diffusive limit to $t^{1/2-\alpha}$.

2.2.2 Water Bridge Monitoring

Nanoscale control of water bridge formation is of fundamental interest, as well as practical concern, for nanocell control in nanolithography. Initial reports of DFM oxidation by Wang et al., in 1994, were performed using feedback ON conditions. Perez-Murano et al., also in 1994, suggested that switching the feedback OFF provided an alternative to voltage switching [20]. Then the conditions required to monitor the formation and maintenance of the nanocell – the water bridge between the tip and substrate – have been explored extensively in work carried out by Perez-Murano and Garcia and their co-workers [20–25].

Garcia and co-workers [21, 22, 24] began investigating voltage-induced meniscus formation in 1998 by monitoring the oscillation amplitude during feedback ON/OFF conditions as DC pulse voltages were applied in noncontact mode. The transitions of oscillation amplitude and tip-sample separation under successive switching of the voltage and feedback are illustrated in Fig. 2.1. Step I illustrates the cantilever oscillation amplitude (points) and tip-substrate separation (dashed line) for normal SPM operating conditions, i.e., voltage OFF, feedback ON. Step II demonstrates the reduction in both parameters under the voltage ON, feedback OFF state. This was interpreted as representing the impact on the cantilever oscillation due to the addition of the electrostatic force between the tip and substrate. Step III indicates that a reduced amplitude condition persists in the voltage OFF, feedback OFF state, although the tip-sample separation increases to an intermediate position between the Step I and Step II positions. This indicates that a water meniscus clearly forms in the

Fig. 2.1 Observation of electrostatic force and water bridge formation during dynamic force oxidation: Cantilever oscillation amplitude as a function of time before, during, and after the formation of an oxide dot. [Source: R. Garcia et al. [21], figure 1. Copyright © American Institute of Physics]



course of Step II, as the original authors conclude. The final step returns the system to the Step I state, increasing the larger oscillation amplitude corresponding to its feedback ON set point value, rupturing the meniscus and returning the tip-substrate separation to its pre-determined value.

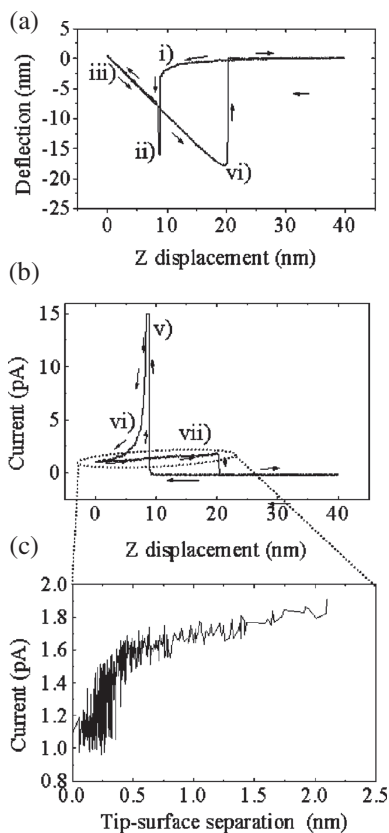
The work by Calleja et al. [24] also investigated the threshold voltage required for the formation of the water bridge. The voltage pulse required to form a water bridge was found to be greater than that for the subsequent oxidation reaction for a given tip-substrate separation. The capacitance between water layers on surfaces of the energized tip and substrate is strongly non-uniform due to the curvature of the tip and this induces a surface tension gradient of these water films. More recent work has included computational efforts under continuum assumptions, i.e., without consideration of ionic concentration and its reorganization and mobility within these films. We examine this question in the following section since it is a critical element for understanding local oxidation in the short-pulse/fast-scan speed limit.

2.2.3 *Combining the Two Concepts*

Although many details of space charge buildup and water bridge formation have been established independently in recent years, there has not been a concerted effort to unify the basic principles articulated above into a coherent understanding of the nanocell, especially under dynamic conditions. This makes it particularly difficult to evaluate various approaches to DFM oxidation and reach a consensus on an entirely optimized methodology for local oxidation. This chapter certainly doesn't provide a final answer. However, in a pair of articles published in 2004 [26, 27] we discussed experiments examining current, capacitance, and charge under contact and noncontact conditions. Here we mention a few conclusions from that work which provides guidance for interpreting already published results, Section 2.3, as well as performing new DFM oxidation experiments, Section 2.4, based on these efforts to intentionally link the space charge and meniscus formation concepts.

Now, the experiment in Fig. 2.1 [21], on its own, provides no information about charge deposited and current flow that actually occurs as voltage is applied through the meniscus. Figure 2.2 presents results reported by us and our colleagues in 2003 [28]. In this work we monitor simultaneously the cantilever deflection and current measurements for a force-distance curve. Note that the voltage is 12 V, 40%RH, 40 N/m. This simple measurement reveals that electrostatic bending of the cantilever occurs until the force overcomes the resistance of the cantilever. At this point in the force curve, a current of about 15 pA flows momentarily through the tip-sample junction and drops off as oxidation takes place. The oxidation reaction persists until the mechanical pull-off force exceeds the attractive surface tension of the nanocell. Prior to pull-off, the attractive force associated with the nanocell reaches a point at which it is no longer in contact with the substrate. What is interesting here is that if we plot the current vs. the actual tip-surface separation (rather than z displacement); we see that current increases from 1 to 2 pA before the meniscus is ruptured. This apparently paradoxical current increase can be explained: By moving the tip out

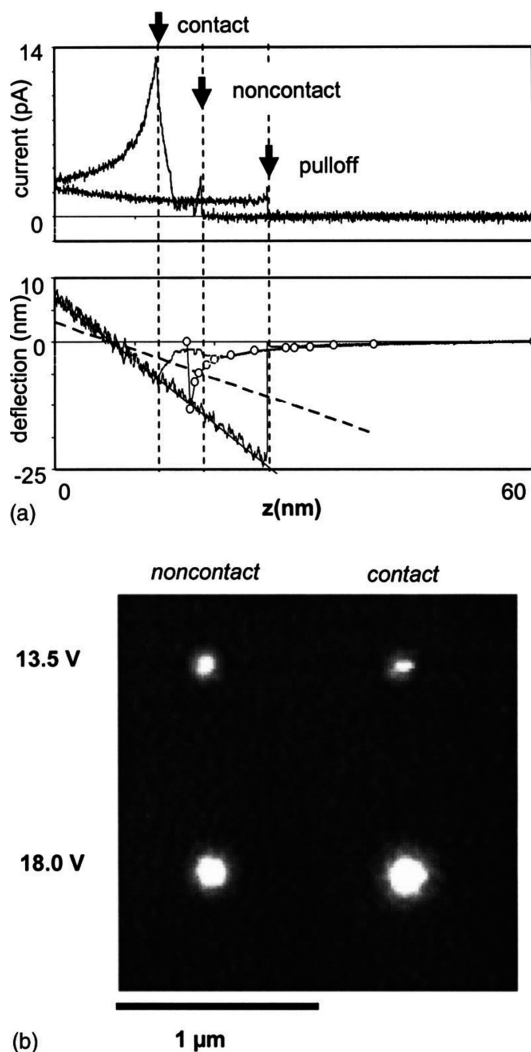
Fig. 2.2 Observation of simultaneous electrostatic cantilever bending and current flow during a force curve (voltage ON, feedback OFF): (a) Cantilever deflection and (b) current as a function of z -displacement. (c) Current as a function of tip-surface separation as the tip retracts from the substrate. Tip-surface separation is the z -displacement plus cantilever deflection. [Source: F. Perez-Murano et al. [28], figure 1. Copyright © American Institute of Physics]



of direct contact with the surface, ionic charge can be reorganized, and thereby reduced, allowing current across the junction to increase.

The measurement illustrated in Fig. 2.2 thus provides a complementary view to the one established in Fig. 2.1 in the sense that the connection between current flow and tip-substrate separation are correlated directly during the approach and retract cycles. Furthermore, the relationship between oxide volume and current can be investigated in detail. Figure 2.3 [27] again demonstrates the necessity of the water bridge but the experiment incorporates an important additional feature: Here oxide growth for identical pulse conditions (13 and 18 V, 1 s) performed under contact and noncontact conditions are compared. Note that the peak current obtained when the tip is in repulsive contact is on the order 10 nA whereas it is on the order of 1 nA if the current flows through a water meniscus. What is indeed interesting about this measurement is that the height, diameter, and volume of the oxide feature produced is nearly identical for the same exposure conditions regardless of whether or not the tip is in direct contact with the substrate. We interpreted this measurement to mean that considerable excess, i.e., non-faradaic, current occurs if the tip is in direct contact with the substrate; in contrast, essentially only faradaic current occurs

Fig. 2.3 (a) Observation of simultaneous electrostatic cantilever bending and current flow during a force curve (voltage ON, feedback OFF) for contact and noncontact force curves. (b) Oxide features patterned in contact and noncontact conditions using identical exposure conditions. [Source: J. A. Dagata et al. [27], figure 5. Copyright © American Institute of Physics]

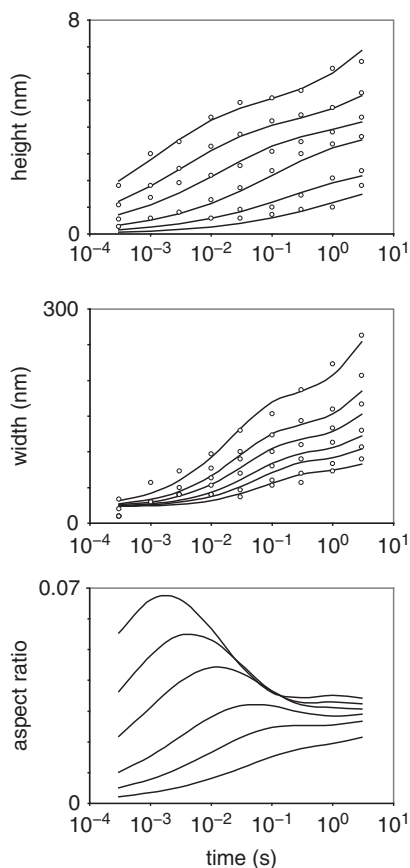


if the tip is connected only through the water meniscus. Since non-faradaic current is either lost or contributes to the production of defects or charge traps within the growing oxide film, the preference for noncontact oxidation becomes obvious.

2.2.4 Water-Bridge Formation at High Voltage

The observation that a threshold voltage exists for the formation of a water bridge between the tip and substrate mentioned earlier was further examined by Calleja et al. [24], in particular, in a set of measurements that examined the effect of high

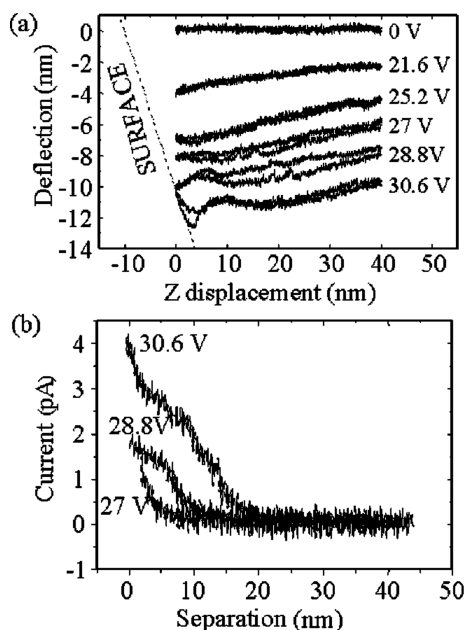
Fig. 2.4 Semi-log plots of oxide height, width, and aspect ratio (height: width) of *dots* formed during feedback OFF DFM oxidation as a function of exposure time. Curves increase in regular voltage increments from low (8 V) to high (24 V) in each panel. Experimental data (circles) from Reference 24, figure 2]. Calculated values (continuous lines) are based on previously published Alberty & Miller rate constants for silicon published in Reference 10



voltage and short exposure time on oxide growth rate for feedback OFF DFM mode. Their conclusion was that high-voltage, short-time pulses provide an advantage when patterning in this mode. In Fig. 2.4, we replot their data – presented as height (h), width (w), and time (t) in Figs. 2.1 and 2.2 of their article – as aspect ratio (h/w) vs. t . These experimental feedback OFF DFM oxidation data are compared to calculated values obtained from the Alberty & Miller kinetic model and rate constant parameters reported in Reference 10. What is interesting is that the applied voltage in this experiment ranged from 8 to 24 V, much higher than the range of voltage usually studied. Our manner of plotting the data reveals the appearance of a distinct maximum in the aspect ratio, at increasingly shorter times, as the applied voltage is increased. Figure 2.4 confirms their conclusion, but offers additional insight into a unique aspect of DFM lithography: The possibility of extremely fast oxidation, albeit if one is willing to accept limited oxide thickness of about 3 nm or so.

The benefits of high-voltage oxidation in DFM do not end with short pulse times. Simultaneous cantilever deflection and current measurements obtained during a force–distance curve using applied voltages in the range of 20 V to 30 V reveal

Fig. 2.5 (a) Cantilever deflection as a function of z-displacement during high voltage noncontact force curves. (b) Current as a function of tip-surface separation measured during a high-voltage, noncontact force curve. [Source: F. Perez-Murano et al. [28], figure 3. Copyright © American Institute of Physics]



that the onset of measurable current – and, hence, spontaneous meniscus formation – occurs even at a tip-sample separation of 20 nm, as indicated in Fig. 2.5. [See the text related to Reference 27, figure 7, and Reference 28, figure 2, for a more detailed discussion.] These results are consistent with the Lippmann equation, which describes the change in surface tension due to a change in surface potential arising from the capacitance of and mobile charges present in the water layers covering the tip and substrate. Extrapolating the results calculated by Garcia-Martin & Garcia to high voltage [29], we find that spontaneous meniscus formation at 20 nm tip-substrate separation is predicted for an applied voltage of 30 V. However, it should be noted that the existence of ions in the water layers cannot be neglected when we account for cyclic oxide formation during large-amplitude feedback ON DFM oxidation.

2.3 Key Concepts in Dynamic-Force Mode Methods

In addition to minimizing space charge effects during oxidation, repeatable and precise control of meniscus shape formation is a crucial element for SPM-based nanolithography. The first DFM oxidation reports performed in feedback ON conditions relied on extremely low set points to avoid instability of feedback operation due to the instantaneous switching of voltage [30]. For arbitrary pattern generation, it is desirable for the SPM system to switch smoothly from imaging mode to lithography mode as the SPM tip is brought into position. This section reviews work

Table 2.1 Parameters reported in selected DFM oxidation approaches (feedback ON)

	Maximum voltage (V)	RH(%)	Substrate	Oxidation time or scan speed	Tip coating / spring constant (N/m)	Oscillation amplitude (nm)
Vicary and Miles [34]	12	60	p-Si:H	2 cm/s	PtIr 42	5
Graf et al. [38]	16	42	n-GaAs	2 $\mu\text{m/s}$	TiPt 40	–
Kuramochi et al. [39]	10	45	p-Si:H	1 $\mu\text{m/s}$	Rh 20	258
Clement et al. [33]	30	70	n-Si:H w/oxide regrowth	2 $\mu\text{m/s}$	– 40	20
Legrand and Stievenard [32]	12	–	Si:H	–	–	12
Fontaine et al. [40]	12		Si:H	10 $\mu\text{m/s}$	PtTi 40	2

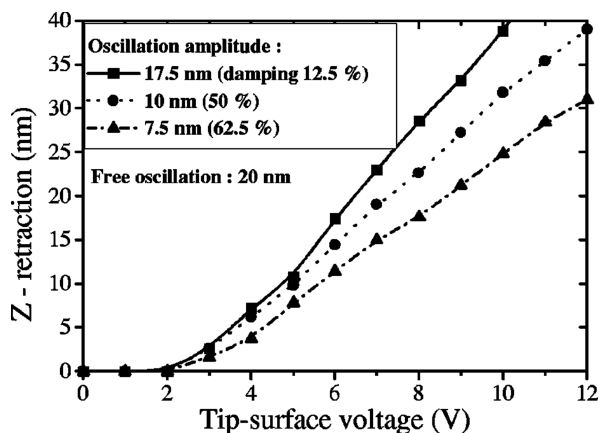
reported in several articles selected from the feedback ON DFM oxidation literature. These articles are listed in the Table 2.1 and were chosen because they specifically address control factors affecting DFM oxidation performance.

2.3.1 Synchronized Pulse, Part I

Voltage modulation (VM), i.e., using a series of unipolar or bipolar pulses, rather than a single continuous one, originated in our initial investigations of space charge buildup during local oxidation. In 1998 we were interested in validating the *interfacial* nature of the space charge as revealed by electrical force microscopy (EFM) measurements of oxide features produced under CM conditions as a function of the doping type and level of silicon substrates [15, 16]. The frequency dependence of the enhancement and the oxide density variation as a function of dopant form a necessary logical connection to the classic literature of low-temperature oxidation [11, 12].

The implication that voltage modulation enhances oxidation by reducing the build up of space charge tested a certain hypothesis. In a more practical sense, it was of interest for producing thicker oxide features and avoiding the slow-growth, steady-state regime and, especially, lateral diffusion that reduced the aspect ratio of oxide features. VM techniques provide an important benefit specific to DFM oxidation, as first described by Legrand & Stievenard in 1999 [31, 32]. Their principal concern was to overcome the old problem of avoiding the discontinuities produced by voltage switching during feedback ON operations. They studied the effect of synchronizing the voltage pulses to coincide with the phase of the cantilever oscillation. The electrostatic force, if applied under instantaneous feedback-on conditions,

Fig. 2.6 Retraction of the z-piezo, or z-displacement, as a function of the bias voltage applied between an SPM tip and substrate. [Source: B. Legrand and D. Stievenard [31], figure 1. Copyright © American Institute of Physics]



induces instability in the mechanical oscillatory behavior of the cantilever. An example of the retraction arising from the application of the electrostatic force is shown in Fig. 2.6 [31]. Adjustment of the phase led to much reduced responses of the amplitude and tip-sample separation as a consequence of the time-averaged electrostatic effects due to modulated voltage waveforms. Figure 2.7 illustrates the control of the oxide height and width on phase and oxide lines produced at alternating phase angles. By controlling the damping of oscillation amplitude and modulation of phase between the pulsed voltages and the mechanical excitation, they showed that it was possible to minimize the electrostatic interaction and heighten the meniscus stability during large-scale patterning. To our knowledge, this work has not been followed up on. Our reasonably extensive exploration of this approach indicated that it produced excellent aspect ratio features once the system parameters were properly tuned; however, we abandoned the technique because of the propensity of a tip to stop oxidizing abruptly and once this happened could not be revived. [This behavior was confirmed by B. Legrand, private communication.]

On the other hand, the insights gained from the approach of Legrand & Stievenard also contributed to our fundamental understanding of balance between electrostatic and meniscus forces during cantilever oscillation, toward a more complete appreciation of the *dynamical* nanocell. This takes us beyond the static picture that feedback OFF characterization of meniscus properties offers.

2.3.2 High Humidity and Fast Scan Speed

In 2003 Clement et al. [33] proposed a novel set of DFM operating parameters, high voltage high humidity and demonstrated high oxidation rates for voltage pulses and relatively fast scan speeds, 2 $\mu\text{m/s}$. They concluded that oxidation rates – height of 1 nm with scan speeds of 1 cm/s could be achieved with DFM oxidation, Fig. 2.8. More recently, Vicary and Miles [34] reported oxidation heights for scan speeds as

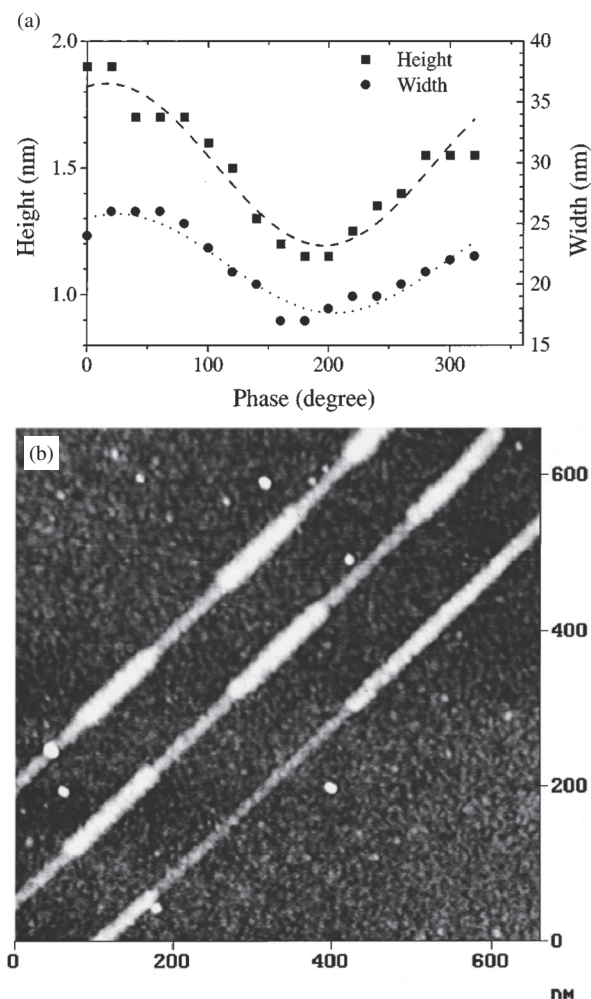


Fig. 2.7 Synchronized pulse DFM oxidation. (a) Variation of the oxide height and width as a function of the phase angle between voltage pulse and cantilever oscillation. (b) Effect of phase modulation on oxide height and width. [Source: B. Legrand and D. Stievenard [32], figures 2 and 3. Copyright © American Institute of Physics]

high as 2 cm/s and single pulse oxidation for times as short as 500 ns, Fig. 2.9. Note that the width or diameter of the oxide features is not an important consideration since these experiments were performed well within the transient region. Parameters for both are listed in the Table 2.1. Note the specific combination of (V , RH , A) – voltage, RH , and cantilever oscillation amplitude values used by Clement et al. (30 V, 70% RH , 20 nm) and Vicary & Miles (12 V, 60% RH , 5 nm) to obtain 1–2 nm of oxide height. Both authors attribute the persistence of the water meniscus as the key explanation for the success of their respective techniques.

Fig. 2.8 SPM topographic image (a) and line profile (b) of oxide dots produced using high-voltage, high humidity DFM oxidation. [Source: N. Clement et al. [33], figure 1. Copyright © 2010 American Vacuum Society]

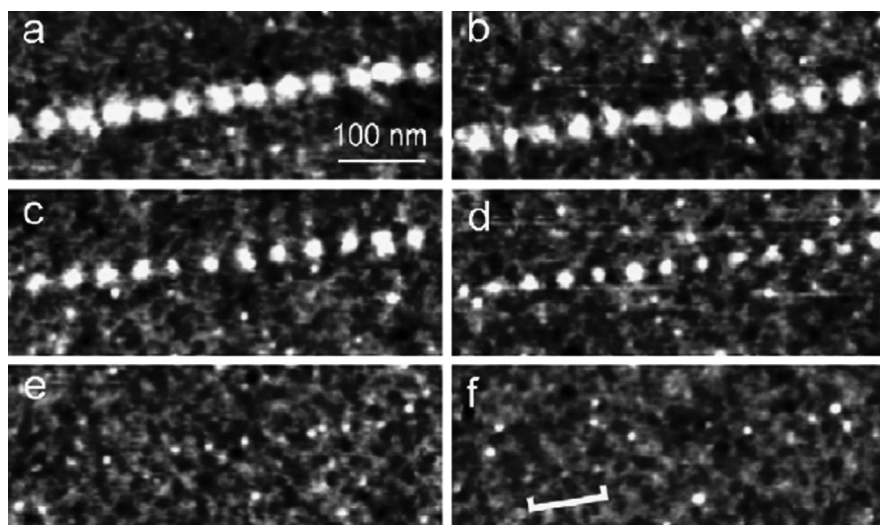
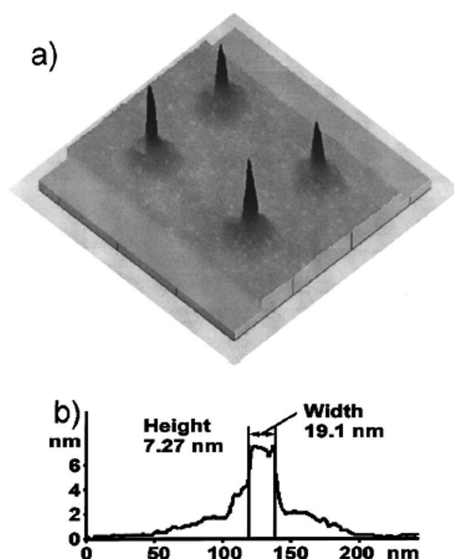


Fig. 2.9 SPM topographic image of *oxide dots* produced using high probe speed DFM oxidation. Exposure time varies from 100 μ s in panel (a) to 500 ns in panel (e). [Source: J. A. Vicary and M. J. Miles [34], figure 2. Copyright © 2010 Elsevier B.V.]

On the basis of our unified concept of the nanocell, we say that all probe-based oxidation follows from the same fundamental process, i.e., that a single process operates from the transient, fast-growth regime, at the transition point, and throughout the steady-state, slow-growth regime. After all, this is what the coupled kinetic

equations of Alberty & Miller are all about. If the fundamentals are shared, it must mean that the (V, RH, A) parameter space allows a reduced RH if A is increased, for instance. Similarly, higher V allows a larger A , and so forth.

These experimental results have been interpreted by the authors by framing the principal question in terms of a “limiting oxidation rate” and “mechanical pressure”. Both Clement et al. and Vicary & Miles chose to pick up the discussion beginning with interpretations given in the work of Snow et al. [35–37] on CM oxidation and Tello & Garcia and co-workers [25] concerning differences between CM and DFM oxidation.

For example, Clement et al. state [33] “Therefore the main difference with the pulsed voltage technique is the higher tip oscillation amplitude combined with high humidity ratio to avoid mechanical pressure during oxide growth and to increase the amount of oxidizing species. This also suggests that oxidizing species are the limiting factor for AFM oxidation.”

The early conclusions of Snow are inconsistent with the space charge model and the view of the nanocell presented earlier. Snow et al. [37] concluded that “...the rate-limiting step of the oxidation process is the production of O anions from the ambient humidity.” This conclusion was based on a clearly erroneous interpretation of data presented in Fig. 2.1 of their paper. As we have shown in Reference 28, figure 6, lateral spreading at high humidity leads to increased oxide feature width – and at the near saturation levels, 95% RH , used in the Snow work – accounts quantitatively for their observations, not condensation from the vapor. Keep in mind that their vapour-to-liquid transition hypothesis was never actually tested. In Reference 29, figure 7 we demonstrate that ionic mobility within the water layers, not condensation from the vapour, explains their results. Current flow through the nanocell is necessary for oxidation, as demonstrated directly in Figs. 2.3 and 2.4. Furthermore, the long-range formation of a water bridge in Fig. 2.5 agrees qualitatively and quantitatively with the capacitance calculations of Garcia-Martin & Garcia [31]. Quite simply, water layers are always present on the tip and substrate surfaces above 20% RH and, if they are not, oxidation does not occur.

Vicary & Miles [34] engage in an equally doubtful line of reasoning in attempting to explain results shown in Fig. 2.2 of their paper: In order to account for the observation that oxide growth ceases entirely for pulse durations longer than 20 μ s, they invoke a model proposed by Tello & Garcia [25] in which the growth rate during CM oxidation is suppressed because of the additional work done by the growing oxide feature to bend the cantilever. [Note, again, that this hypothesis has never been tested experimentally.] The idea applied to the DFM case is that, due to the short duration of the cantilever oscillation and oxidation pulse in their experiments, the feedback loop does not raise the tip in response to the growth of oxide. The difficulty with this reasoning is that it ignores the degrees of freedom that oxyanions possess in the nanocell – and here we specifically include lateral diffusion within both the water meniscus and the oxide. In the nanocell, anions are not constrained by a fixed boundary, rather, they respond by diffusing laterally, a dissipative mechanism at the heart of the space-charge concept.

2.3.3 Synchronized Pulse, Part II

Graf et al. [38] tried optimizing the ratio of oxidation time to total pulse cycle in their approach to voltage modulation during feedback ON DFM oxidation of Ga[Al]As and n-Si. To achieve the most stable and efficient lithographic conditions, these authors suggested that it is necessary to determine an effective oxidation time ratio for the system. They found that the feedback ON DFM requirement of operating with a low set point, i.e., $8\% < \text{DC set} < 16\%$ of the free oscillation amplitude, as others had reported, could be substantially increased to a range of $10\% < \text{VM set} < 40\%$, because the time averaged electrostatic force experienced by the feedback loop is reduced, similar to the reasoning of Legrand & Stievenard [31], however, without the additional step of exactly synchronizing the voltage pulse and cantilever oscillation.

Another interesting result that they report is one bearing directly on the question of comparative reliability of VM versus DC exposure for feedback ON DFM oxidation. The series of lines shown in the SPM image of Fig. 2.10 are representative

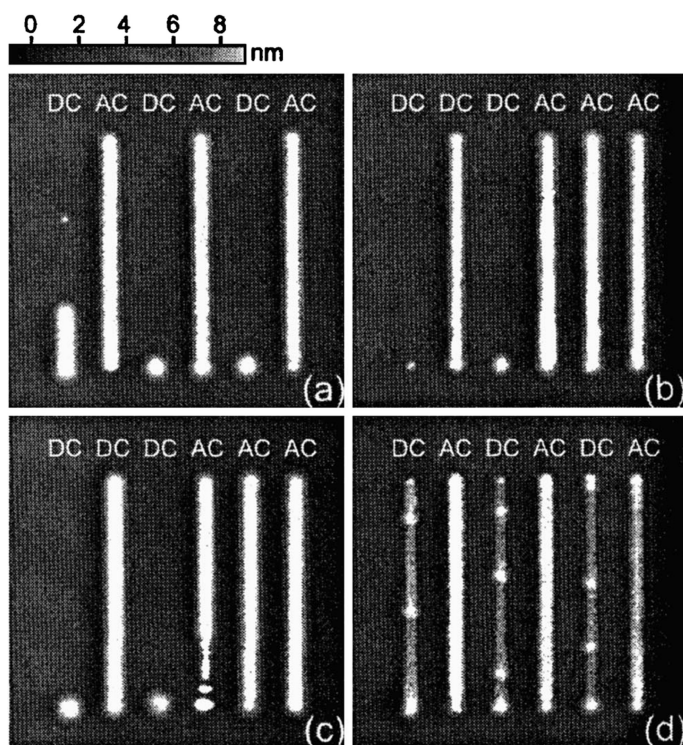


Fig. 2.10 Comparative reliability of DC and voltage modulation, referred to as VM in the text and labeled AC in the figure. SPM topographic image presents alternating series of oxide lines produced by DFM oxidation on undoped GaAs. [Source: D. Graf et al. [38], figure 5. Copyright © American Institute of Physics]

of a much larger set of exposures. As Graf et al. [38] note “In ac oxidation we have the chance to pick up the water film in each cycle. . . in the *dc* mode, however, once it failed at the beginning, the strong additional electrostatic damping will keep the tip too far from the sample surface for a water bridge to form.” By operating in a pulsed mode situation, even an inevitable disruption of the nanocell can be repaired on the following voltage cycle. We gradually become aware of the possibility that a persistent meniscus is not actually necessary for reliable DFM oxidation. In other words, it may be essential for a stable feedback loop, but not for lithography. As we demonstrate shortly, the persistence of the meniscus is not even needed for that.

These authors also explore another aspect of practical concern to DFM oxidation in their comparative study of the breakdown voltage of DC and VM oxide lines. The density and electrical properties of oxide features are crucial to their performance as prototype etch masks and device structures. To study the voltage breakdown of DC and VM lines, they defined the elements of a Ga[Al]As two-dimensional electron gas (2DEG) device is shown in Fig. 2.11a, with DC isolation patterned in the

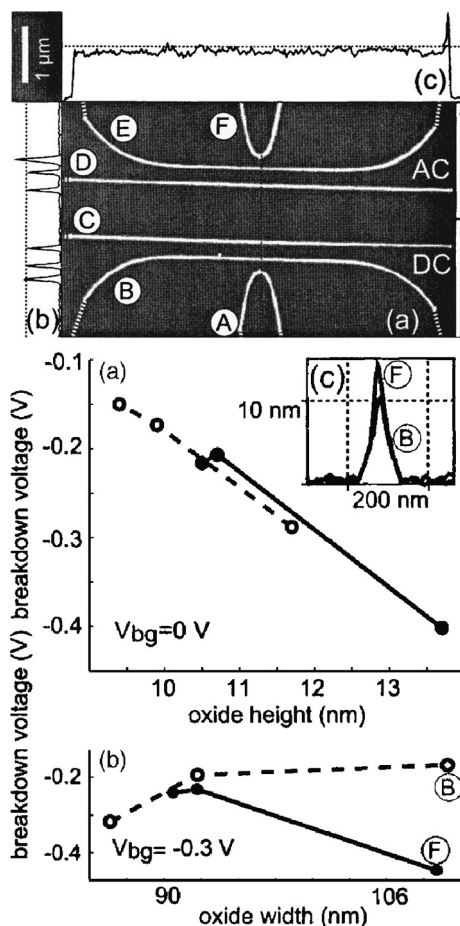


Fig. 2.11 (a) SPM topographic image of a GaAs 2DEG test device with lines fabricated by DC (lower half) and VM (upper half) DFM oxidation. (b) Comparison of oxide breakdown voltage for DC and VM DFM oxide lines. [Source: D. Graf et al. [38], figures 6 and 7. Copyright © American Institute of Physics]

lower half and VM isolation patterned in the upper half of the overall structure. A breakdown threshold corresponding to 10 pA was determined for each oxide line in the series and plotted in Fig. 2.11b. They attribute the substantial increase of 186% in breakdown voltage to the more uniformly continuous nature of the VM-patterned oxide. While the authors conclude that the final confinement potential of each region of the test device is comparable for DC and VM methods – in doing so they attach more significance to the magnetoresistive results than to oxide quality directly – it is useful to generalize from the special case of remote 2DEG patterning to other device applications.

Voltage breakdown and oxide homogeneity may be far more important metrics for silicon-oxide tunnel barriers or anisotropic etch resistance, for example. It is worthwhile to mention that some years ago we also examined the density variation for local silicon-oxide device structures patterned by DC and VM techniques [18]. Furthermore, annealing effects on the oxide density and interfacial defect density of the oxide features were pointed out and the reduction of such defects produced during the patterning of device structures by local oxidation is necessary in order to achieve acceptable device performance in these systems.

2.4 New Aspects of Reaction Control by Probe Speed

This section sheds new light on achieving the highest possible reliability, writing speed, and large-scale precision through simultaneous analysis of oxide-volume and current-flow measurements during DFM oxidation. We have already reviewed the formation of the nanocell on the basis of investigations in the feedback OFF condition in the foregoing section. While certainly adequate for gaining deeper understanding of the underlying kinetic process, operating in this mode limits patterning to single point-like features which is unsuitable for the practical applications of interest here.

It is for this reason that we focus our attention on feedback ON DFM in the rest of this chapter. Furthermore, we evaluate CM and feedback ON DFM oxidation as an explicit function of probe speed, v , during fabrication of continuous oxide lines and area features [39–45]. Since probe speed is more complicated than a simple inversion of time in the case of VM feedback ON DFM oxidation, when “time” is discussed in the following, a careful distinction between voltage-pulse duration and meniscus-formation cycles [39] must be made. Such a distinction does not arise for CM oxidation of course.

2.4.1 *Small and Large Amplitude*

Most of the authors of articles listed in the Table 2.1, Legrand & Stievenard, Fontaine et al., Vicary & Miles, and Graf et al., have emphasized how the stability of the cantilever oscillation depends on selecting a small value of the oscillation amplitude and a low amplitude set point during feedback ON DFM oxidation. By contrast, we and our colleagues have shown that there is another way to look at the

DFM control problem – by using DC voltage but working at a very *large amplitude*. Cyclic meniscus formation was also found to occur when oxidation was performed with the cantilever driven at high oscillation amplitudes and constant DC voltage was applied. This is comparable to performing oxidation using pulsed voltages. We found that during that part of the cycle when the tip-sample separation is smallest, the meniscus length is essentially constant for fixed voltage and *RH* from cycle to cycle. Thus a meniscus could be formed periodically at large amplitude settings (>200 nm). In this case, since maintaining feedback in its active state is possible under these conditions, we can avoid electrostatic damping, and that as the probe tip makes its closest approach to the substrate, a water meniscus is regenerated as it would be in the case of a voltage pulse. Meniscus lifetime could be controlled to sub-microsecond order by adjusting the cantilever amplitude setting or by modulating its oscillation amplitude by altering the probe-sample distance as illustrated in Fig. 2.12 [23]. This regeneration is both spontaneous and more reliable as revealed in the foregoing sections.

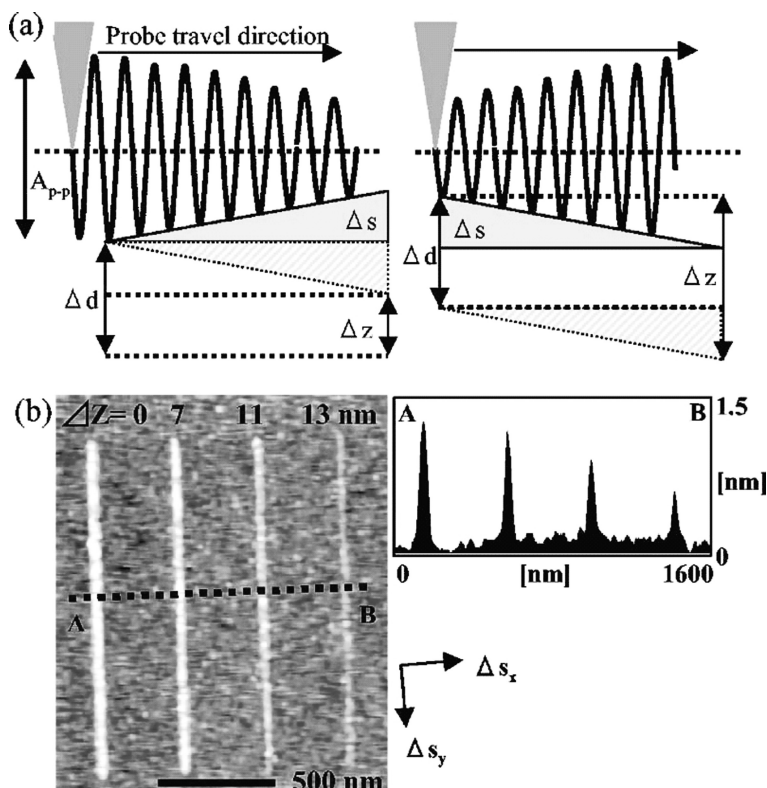


Fig. 2.12 Large-amplitude dynamic force mode oxidation. (a) Decrease of the cantilever oscillation amplitude, $\Delta z = \Delta d - \Delta s$, calculated from the z -piezo displacement, Δd , and the slope of the substrate, Δs . When used in the feedback OFF condition, the minimum oscillation amplitude necessary for stable meniscus rupture may be obtained. [Source: H. Kuramochi et al. [39], figure 1. Copyright © American Institute of Physics]

2.4.2 Comparison of Contact and Dynamic Force Mode Oxidation

Efforts to employ feedback ON DFM oxidation have proceeded in parallel with feedback OFF investigations. Figure 2.13 reproduces early results from Fontaine et al. comparing oxide growth rate for CM and feedback ON DFM oxidation as a function of probe speed [40]. The general trends are that the oxide height, or thickness, and the maximum probe speed that can be used for DFM are somewhat less than for CM, although the voltage-dependent slopes are similar. Note also that the oscillation of the cantilever is set to a remarkably low value of 2 nm in these experiments.

What we now wish to examine is how current and volume calculated for CM and DFM vary in such measurements. Moreover, we want to determine if rupturing and reforming the nanocell during each oscillation cycle of the probe tip – *large-amplitude* DFM lithography – produces a qualitatively similar oxide as low-amplitude DFM lithography. For this purpose, comparative CM and DFM experiments were carried out. Lithographic patterning was performed using an environmental control SPM unit at a constant relative humidity of 50% at room temperature. Probe speed was varied over a range of 0.1–20 $\mu\text{m/s}$. A hydrogen passivated p-type Si(001) sample ($1 - 10 \Omega \cdot \text{cm}$) was used as the sample. Rh-coated Si cantilevers for CM ($\sim 0.1 \text{ N/m}$), for DFM ($\sim 20 \text{ N/m}$) and modified cantilevers

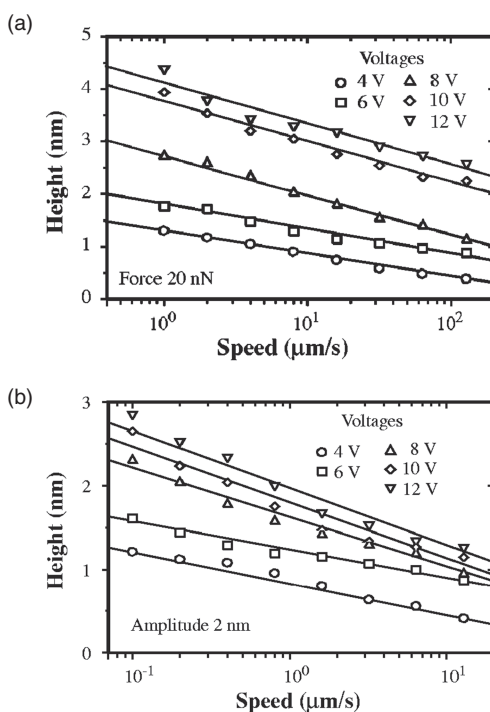


Fig. 2.13 Comparison of contact mode and dynamic force mode oxidation as a function of probe speed: (a) Oxide line height by CM. (b) Oxide line height by DFM. [Source: P. A. Fontaine et al. [40], figures 10 and 17. Copyright © American Institute of Physics]

(~ 3 N/m) with a conductive multi-walled CNT (MWNT) are employed. CNT probes were also used in DFM operation; hereafter experiments with CNT probes were called CNT. The oscillation amplitude set point was maintained at ~ 250 nm (DFM) and less than 10 nm (CNT) during nano-oxidation by maintaining active feedback control. Oxide production was decided by faradaic current detection and visual evaluation of SPM topographic and/or current images.

The effect of probe speed on the line width, volume, and current are summarized in Fig. 2.14. The decrease in average value of the width (FWHM), height and volume of the fabricated oxide lines with increasing probe speed are plotted in Fig. 2.14a–c. The volume of oxide features is standardized as all oxide lines have the same length of 1 μm . Lines in the graphs are to guide the eye. A large decrease in width and volume occurred with increasing probe speed for $v < 1$ $\mu\text{m/s}$. In the region of $v > 1$ $\mu\text{m/s}$, decreases in width and volume of oxide lines were slight. The amount of detected current was found to be in good agreement with the value of ionic charge calculated from the oxide volume for all experimental comparisons, indicating that the detected current was indeed the faradaic current. The faradaic current per unit time increased proportionally with probe speed at low probe speed and became virtually constant at $v = 10$ $\mu\text{m/s}$, as shown in Fig. 2.14d.

Similar experiments employing CM operating mode, Fig. 2.14e–h, and CNT probe tips, Fig. 2.14i–l, were performed under similar exposure conditions. The quantitative properties are basically similar to that in the case of DFM, thicker lines were fabricated at the slower speed and current per unit time increased at higher probe speed in good agreement with the results of Fontaine et al.

The maximum probe speed of 20 $\mu\text{m/s}$ employed here is not the threshold speed for CM exposure. It depends strongly on the RH and material properties of the tip and substrate. Snow and Campbell succeeded fabricating oxide lines at probe speeds up to 1 mm/s on a H-passivated Si(100) surface [35]. Does DFM oxidation possess a corresponding threshold – and what does it mean physically? We will attempt to address this question next.

In the case of CNT probe tips, the applied sample voltage of 8 V is the maximum value that can be applied without damaging the welded attachment of the MWNT to the Si cantilever [46]. The width and normalized volume of the fabricated oxide lines were somewhat less than in the case of DFM fabrication. It is notable that making an entirely continuous line became difficult at $v > 5$ $\mu\text{m/s}$ in the case of a CNT probe tip. Compared to our previous experience with RH dependence of DFM oxidation conditions, discontinuous fabrication is a result of poor meniscus formation, i.e., water deficiency, arising from the hydrophobicity of CNT probe tips. The hydrophobicity made the length of the water short, therefore, meniscus formation was cyclic, similar to the large-amplitude case, although the amplitude set point was smaller.

By normalizing the faradaic current density in terms of the oxide volume for the CM, DFM, and CNT datasets presented in Fig. 2.15a, we find that the progression of oxide formation for all three operating conditions follows a common path as shown in Fig. 2.15a. However, there is a key difference that distinguishes these three operating conditions, namely an effective time factor for oxidation – the time

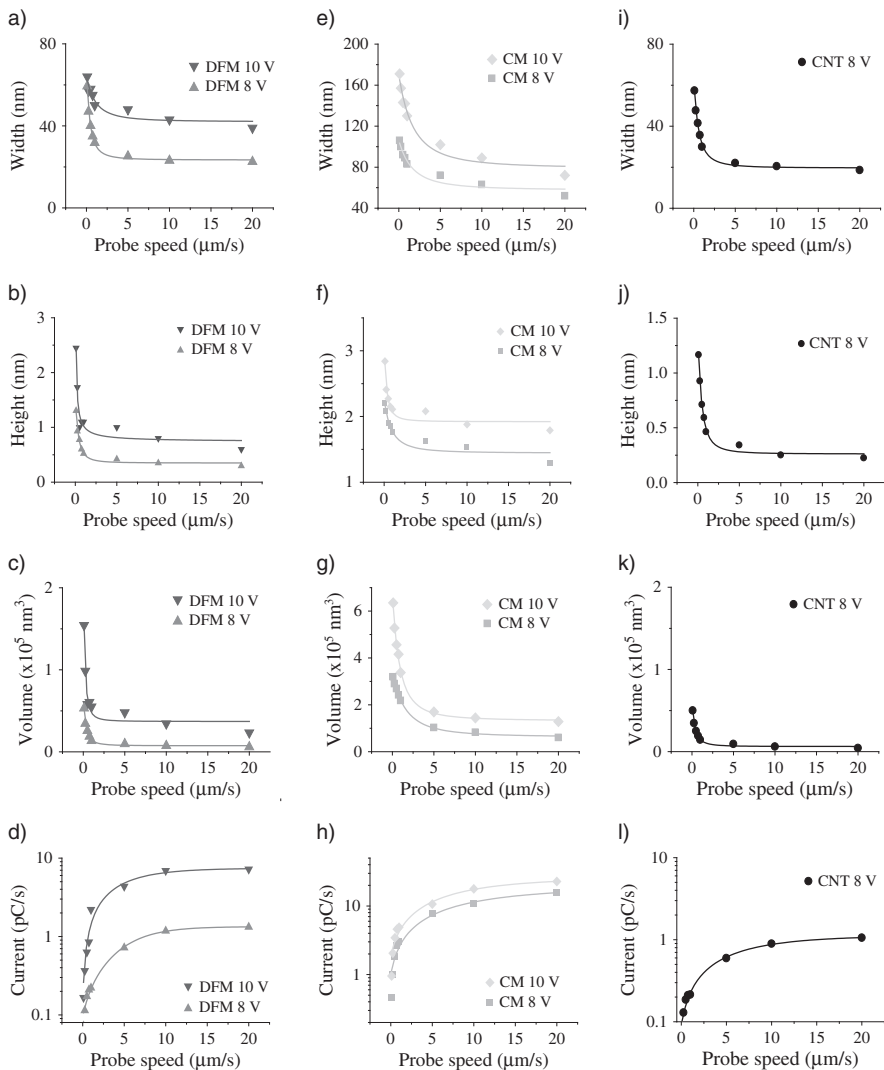


Fig. 2.14 Effects of probe speed on oxide volume and detected faradaic current in DFM (a)–(d), CM (e)–(h) and CNT (i)–(l) nano-oxidation. Oxide width with an accuracy of ± 2 nm (a), (e), (i), and the volume (c), (g), (k) decreased when the probe speed increased under all conditions. The measurement errors in the width and height made the error in volume less than 10%. By contrast, detected current (d), (h), (l) increased with the increment of probe speed. The original detection limit of the current amplifier is ~ 50 fA

factor directly reflects the interplay of oxide growth kinetics and the cyclic nature of the water meniscus for large-amplitude DFM oxidation. Since the voltage pulse duration and humidity effect are strongly coupled to the rates of ionic diffusion and meniscus life time [26, 27, 39, 41, 43, 44], the growth mechanism must be

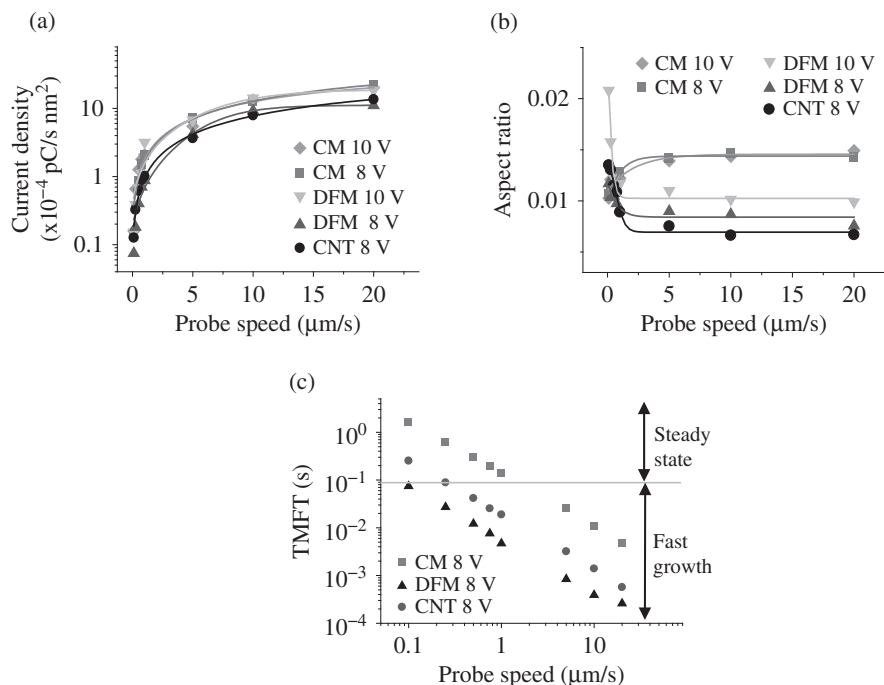


Fig. 2.15 (a) Effects of probe speed on detected faradaic current density. The error is less than 10%. (b) Effects of probe speed on aspect ratio. The error is less than 10%. (c) Relationship between probe speed and total meniscus formation time (TMFT). The border line indicates the transition point at $RH = 50\%$ and $V_s = 8$ V. If the plot point is below the line, the oxidation state is in the fast growth regime

considered as a two step process according to the role of the space charge [15, 16, 42, 43], i.e., the transient-growth and steady-state regimes. Recall that in the latter, surface ionic diffusion due to the low ionic mobility inside the oxide causes the oxide shape to change: The narrow center part of the oxide feature is built up during the initial high growth stage, followed by a lateral expansion rate that overtakes the vertical growth rate during the steady state growth stage. Under the present experimental conditions for which $RH = 50\%$, the humidity effect does not yet appear obvious [44], but surface ionic diffusion definitely occurs as space charge persists for longer and longer exposure times.

The role of cyclic meniscus formation becomes apparent by replotting these data in Fig. 2.15b, *aspect ratio vs. probe speed*, as we did earlier for DFM voltage pulses in Fig. 2.4, *aspect ratio vs. time*. Figure 2.15b also indicates a crossover from steady state growth conditions at low probe speed to transient growth conditions at high probe speed. In the case of CM oxidation, the aspect ratio *increases* somewhat with increasing v to become almost constant at high probe speed for probe speed above $5 \mu\text{m/s}$; conversely, the contribution of lateral oxide growth to total oxide volume production is significant at low probe speed. By contrast, the aspect ratio *decreases*

with the increase in probe speed in the case of DFM and CNT oxidation because vertical oxide growth continues during repeated oxidation of the same surface area – the system remains in the transient regime. The explanation is that meniscus formation is cyclical, the effective oxidation time is very short in DFM, and the oxidation reaction terminates for a portion of every oscillation cycle before lateral ionic diffusion occurs [43]. Moreover, as the probe tip is displaced in response to the voltage pulse, water flows onto the fabricated oxide, which is considerably more hydrophilic than the surrounding H-passivated Si surface. Water condensation is thus confined to a narrow region of the meniscus directly beneath the probe tip and oxidation at the base of the meniscus is suppressed.

2.4.3 Concept of the Total Meniscus Formation Time

As noted earlier, the first detailed investigations of DFM oxidation were performed under greatly reduced oscillation amplitude of the cantilever. Careful monitoring of the amplitude is necessary to ensure stable meniscus formation during voltage switching. Both the work of Garcia et al., Fig. 2.1, and Fontaine et al., Fig. 2.13, employed small oscillation amplitude, i.e., under feedback OFF and feedback ON DFM oxidation, respectively. The results shown in Figs. 2.12, 2.14 and 2.15 indicate that operating with such small oscillation amplitudes is not necessary.

However, operating successfully in the large-amplitude regime requires a separate analysis of cyclic meniscus formation since the physical situation is qualitatively different from the small-amplitude case. In this sense, feedback OFF DFM oxidation is more akin to CM exposure since the meniscus remains intact for the entire length of the voltage pulse. Thus we can define a *total meniscus formation time* (TMFT) at a given location on the substrate to be d ms. (Consider that if the probe speed is set at $1\text{ }\mu\text{m/s}$, a meniscus of diameter d nm exposes a certain minimum area at a single location on the substrate for a duration of d ms.) But the TMFT for large-amplitude DFM exposure depends also on the oscillation frequency of the cantilever and the amplitude set point – the cyclical existence of a meniscus and therefore the propensity for oxidation through the nanocell and so may be quite different [17, 18].

To make an estimate of such difference, we may assume that the oscillation of the cantilever is harmonic. For example, using resonant frequencies of 110 and 150 kHz, setting amplitudes of 250 and 5 nm, and a meniscus length of 8 and 2 nm for DFM and CNT cases [41, 46], respectively, then the meniscus formation time may be estimated to be about 0.83 and 1.97 μs , respectively. TMFTs calculated for these exposure conditions follow a power-law relationship as shown in Fig. 2.15c. Now if oxidation exposure occurs continuously at a given substrate location, the growth rate decreases due to the buildup of space charge. The transition point is about 0.09 s for typical values of $RH = 50\%$ $V_s = 8\text{ V}$ for CM oxidation [42].

On the other hand, if the TMFT is less than the transition point, the reaction state remains in the fast growth regime as confirmed by the single-exponential fit to the data in Fig. 2.15c, exposure conditions for DFM mode correspond to the fast

growth regime. In the CNT case, $v = 0.25 \mu\text{m/s}$ is just on the boundary between fast and slow growth conditions. If we want to operate CM oxidation in the fast growth regime, the probe speed must be set to $5 \mu\text{m/s}$ or higher. This trend is similar to that of the humidity effect in CM, DFM and CNT cases [43]. Operation in the fast growth regime improves reproducibility in the size and shape of oxide features since variability due to ionic diffusion is reduced. Now it is clear that we can control the reaction state by the probe speed.

2.5 Conclusion: Toward Higher Reliability and Efficiency

From a practical standpoint, quality of the oxide feature and performance of the process have primary importance. Not only the final accuracy of the fabrication, i.e., pattern placement and aspect ratio, but also the reproducibility, stability, and energy efficiency of the underlying process must be continuously refined. The role of the most obvious control factors – (V , RH , t) – have become standard parameters reported by all authors in the field. Through this reporting we gain a sense of the “typical” range of the values employed in the published literature and thus are in a better position to assess potential benefits of applying unusually large voltages or very high RH . Then, on the other hand, there are examples that point to an effective combination both large V and RH , as shown in the work of Fontaine et al. [40]. However, not all of these factors can at once be established in every experimental situation, leading to confusion over an optimized choice of parameters to employ in practical processing conditions. And this is why we need to develop an adequate understanding of the full range of possibilities available with DFM oxidation. Then the question rests on how to incorporate the insight from demonstrations of fast scan/small amplitude by Vicary & Miles for instance with our novel approach which shows that it is not essential for cantilever stability if the meniscus doesn’t really remain intact.

Our own view emphasizes that monitoring faradaic current and understanding the existence of charged ions in the water layers, prior to and during the spontaneous formation of the water bridge are essential facts that account for the large-amplitude oxidation results during feedback ON DFM. As we have shown, this ultimately reduces uncertainty in feature size and increases reliability for large-scale patterning of fine features. It should be noted that measuring faradaic current in the case of high conductivity samples may not always be possible. In this case, relying on effective exposure “time” estimates calculated from the TMFT, although not exact, nevertheless provides a guide to suppressing lateral ionic diffusion and achieving higher aspect ratio and enhanced reproducibility. An important feature of TMFT is that it can be controlled externally by setting the *dynamic* operating parameters of the SPM instrument, namely, the resonance frequency, amplitude of the cantilever, RH , probe-sample distance and probe speed.

Energy efficiency is another important practical aspect of exposure control. The highest energy efficiency is achieved when the oxidation rate is maintained just below point at which the transition to lateral ionic diffusion becomes significant

and oxidation remains in the fast growth regime as long as possible. Direct faradaic current detection during CM oxidation at a fixed point under actual process condition is the best way to determine this transition point. It is also possible to estimate it by a calculation of the growth rate from the oxide volume production. The DFM oscillation and probe speed can then be adjusted so that TMFT occurs just before the transition point. This is possible because very rapid, cyclic meniscus formation in high-amplitude DFM operation mode is more precisely controllable than voltage pulses defined solely in terms of time.

This chapter has attempted to bring together the more familiar aspects of the electrochemical nanocell with a critical discussion of feedback ON DFM oxidation. Future progress of local oxidation demands that novel refinements of these methods be investigated and the full implication for faster, more reliable operation uncovered and reported. Finally, let us express our hopes that such gains in processing efficiency will eventually find their way into truly high-throughput extensions of local oxidation, e.g., high-voltage nanoimprint lithography [46, 47] or parallel cantilevers [48].

References

1. J. A. Dagata, J. Schneir, H. H. Harary, C. J. Evans, M. T. Postek and J. Bennett, *Appl. Phys. Lett.* **56**, 2001 (1990).
2. A. A. Tseng, A. Notargiacomo and T. P. Chen, *JVST B* **23**, 877 (2005).
3. D. Stievenard and B. Legrand, *Prog. Surf. Sci.* **81**, 112 (2006).
4. J. A. Dagata, in *Scanning Probe Microscopy: Electrical and electromechanical phenomena at the nanoscale*, edited S. Kalinin and A. Gruverman, Springer Press, New York (2007), Vol. II, p. 858.
5. A. Orians, C. B. Clemons, D. Golovaty and G. W. Young, *Surf. Sci.* **600**, 3297 (2006).
6. S. Djurkovic, C. B. Clemons, D. Golovaty and G. W. Young, *Surf. Sci.* **601**, 5340 (2007).
7. A. Plonka, *Prog. React. Kinet.* **16**, 157 (1991).
8. R. Meltzer and J. Klafter, *Phys. Rep.* **339** 1 (2000) and references therein.
9. R. A. Alberty and W. G. Miller, *J. Chem. Phys.* **26**, 1231 (1957).
10. J. A. Dagata, F. Perez-Murano, G. Abadal, K. Morimoto, T. Inoue, J. Itoh, K. Matsumoto and H. Yokoyama, *Appl. Phys. Lett.* **76**, 2710 (2000).
11. H. H. Uhlig, *Acta Metall.* **4**, 541 (1956).
12. F. P. Fehlner and N. F. Mott, *Oxid. Met.* **2**, 59 (1970).
13. D. R. Wolters and A. T. A. Zegers-van Duynhoven, *J. Appl. Phys.* **65**, 5126 (1989).
14. E. Dubois and J.-L. Bubendorff, *J. Appl. Phys.* **87**, 8148 (2000).
15. J. A. Dagata, T. Inoue, J. Itoh and H. Yokoyama, *Appl. Phys. Lett.* **73**, 271 (1998).
16. J. A. Dagata, T. Inoue, J. Itoh, K. Matsumoto and H. Yokoyama, *J. Appl. Phys.* **84**, 6891 (1998).
17. F. Perez-Murano, K. Birkelund, K. Morimoto and J. A. Dagata, *Appl. Phys. Lett.* **75**, 199 (1999).
18. K. Morimoto, F. Perez-Murano, and J. A. Dagata, *Appl. Surf. Sci.* **158**, 205 (2000).
19. C. R. Kinser, M. J. Schmitz, and M. C. Hersam, *Adv. Mater.* **18**, 1377 (2006).
20. F. Perez-Murano, G. Abadal, N. Barniol, X. Aymerich, J. Servat, P. Gorostiza and F. Sanz, *J. Appl. Phys.* **78**, 6797 (1995).
21. R. Garcia, M. Calleja and F. Perez-Murano, *Appl. Phys. Lett.* **72**, 2295 (1998).
22. M. Calleja, J. Anguita, R. Garcia, K. Birkelund, F. Perez-Murano and J. A. Dagata, *Nanotechnology* **10**, 34 (1999).

23. R. Garcia, M. Calleja and H. Rohrer, *J. Appl. Phys.* **86**, 1898 (1999).
24. M. Calleja and R. Garcia, *Appl. Phys. Lett.* **76**, 3427 (2000). We thank RG for providing the data in Figure 4 in numerical form.
25. M. Tello and R. Garcia, *Appl. Phys. Lett.* **79**, 424 (2001).
26. J. A. Dagata, F. Perez-Murano, C. Martin, H. Kuramochi and H. Yokoyama, *J. Appl. Phys.* **96**, 2386 (2004).
27. J. A. Dagata, F. Perez-Murano, C. Martin, H. Kuramochi and H. Yokoyama, *J. Appl. Phys.* **96**, 2393 (2004).
28. F. Perez-Murano, C. Martin, N. Barniol, H. Kuramochi, H. Yokoyama and J. A. Dagata, *Appl. Phys. Lett.* **82**, 3086 (2003).
29. A. Garcia-Martin and R. Garcia, *Appl. Phys. Lett.* **88**, 123115 (2006).
30. D. Wang, L. Tsau and K. L. Wang, *Appl. Phys. Lett.* **65**, 1415 (1994).
31. B. Legrand and D. Stievenard, *Appl. Phys. Lett.* **76**, 1018 (2000).
32. B. Legrand and D. Stievenard, *Appl. Phys. Lett.* **74**, 4049 (1999).
33. N. Clement, D. Tonneau, B. Gely, H. Dallaporta, V. Safarov, and J. Gautier, *JVST B* **21**, 2348 (2003).
34. J. A. Vicary and M. J. Miles, *Ultramicroscopy* **108**, 1120 (2008).
35. E. S. Snow and P. M. Campbell, *Appl. Phys. Lett.* **64**, 1932 (1994).
36. E. S. Snow, P. M. Campbell, and F. K. Perkins, *Appl. Phys. Lett.* **75**, 1476 (1999).
37. E. S. Snow, G. G. Jernigan, and P. M. Campbell, *Appl. Phys. Lett.* **76**, 1782 (2000).
38. D. Graf, M. Frommenwiler, P. Studerus, T. Ihn, K. Ensslin, D. C. Driscoll and A. C. Gossard, *J. Appl. Phys.* **99**, 053707 (2006).
39. H. Kuramochi, K. Ando, T. Tokizaki and H. Yokoyama, *Appl. Phys. Lett.* **88**, 093109 (2006).
40. P. A. Fontaine, E. Dunois and D. Stievenard, *J. Appl. Phys.* **84**, 1776 (1998).
41. H. Kuramochi, K. Ando, T. Tokizaki and H. Yokoyama, *Jpn. J. Appl. Phys.* **45**, 2018 (2006).
42. H. Kuramochi, F. Perez-Murano, J. A. Dagata and H. Yokoyama, *Nanotechnology* **15**, 297 (2004).
43. H. Kuramochi, T. Tokizaki, H. Yokoyama and J. A. Dagata, *Nanotechnology* **18**, 135703 (2007).
44. H. Kuramochi, K. Ando and H. Yokoyama, *Surf. Sci.* **542**, 56 (2003).
45. H. Kuramochi, K. Ando, T. Tokizaki and H. Yokoyama, *Appl. Phys. Lett.* **84**, 4005 (2004).
46. A. Yokoo, *JVST B* **21**, 2966 (2003).
47. M. Cavallini, P. Mei, F. Biscarini and R. Garcia, *Appl. Phys. Lett.* **83**, 5286 (2003).
48. D. Wouters and U. S. Schubert, *Nanotechnology* **18**, 485306 (2007).



<http://www.springer.com/978-1-4419-9898-9>

Tip-Based Nanofabrication
Fundamentals and Applications

Tseng, A.A. (Ed.)

2011, X, 466 p., Hardcover

ISBN: 978-1-4419-9898-9